6.4 THE INFLUENCE OF LOW-LEVEL STABLE LAYERS ON DAMAGING SURFACE WINDS WITHIN BOW ECHOES

Nolan T. Atkins and Jonathan J. Cunningham
Lyndon State College, Lyndonville, Vermont

1. INTRODUCTION

Bow echoes are a well-known mode of severe convection capable of producing long swaths of straight-line wind damage and tornadoes (Fujita 1979). The straight-line wind damage swaths may be created by the rear inflow jet (RIJ) descending to the ground near the apex of the bow echo behind the gust front (Fujita 1978). Recent modeling and observational studies (Trapp and Weisman 2003; Atkins et al. 2005; Wakimoto et al. 2006a; Wheatley et al. 2006) have shown that low-level (0-3 km AGL), small-scale (1-10 km) "mesovortices" formed on the bow echo gust front are also capable of producing the straight line wind damage swaths. Mesovortices also serve as the parent circulations for tornadoes within bow echoes (e.g., Przybylinski et al. 2000; Atkins et al. 2004; Atkins et al. 2005).

The spatial extent and severity of surface wind damage can vary markedly within bow echoes. Damage surveys by Fujita (1978) documented bow echo damage swaths of a couple hundred kilometers in length that contained F2 damage. On the other hand, recent observational studies by Wakimoto et al. 2006b and Jorgensen et al. (2006) have presented detailed airborne Doppler radar data of mature bow echoes that produced only weak or no damage. In particular, Jorgensen et al. (2006) speculated that low-level stable layers, when present, may inhibit the RIJ from descending to the ground and thus reduce the damage potential within bow echoes.

In this study, we test the hypothesis that low-level stable layers may inhibit the production of damaging surface winds within bow echoes. This will be done by examining idealized simulations produced by the Advanced Research Weather Research and Forecast (ARW) model (Skamarock et al. 2005) of bow echoes interacting with low-level stable layers. The experimental design will be discussed in section 2. An overview of

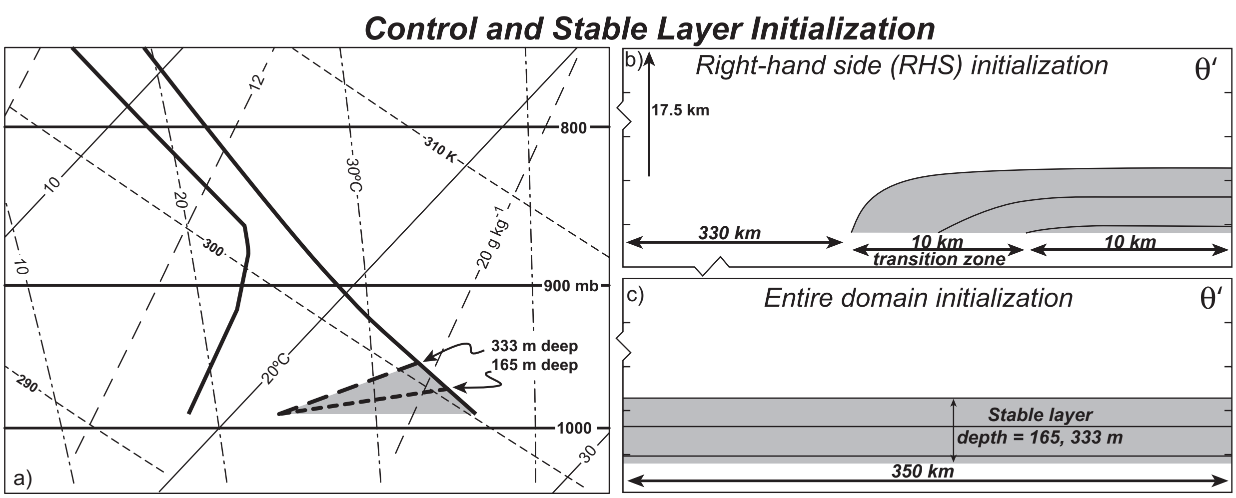

Figure 1. (a) Low-level depiction of the sounding used to initialized the model domain. The stable layer depth and strength is indicated in gray. (b) and (c) Schematic vertical cross sections illustrating how the stable layer is placed in the model domain. The stable layer in indicated by the gray shading.

**Corresponding Author Address*: Dr. Nolan T. Atkins, Department of Meteorology, Lyndon State College, Lyndonville, VT 05851; email: nolan.atkins@lyndonstate.edu

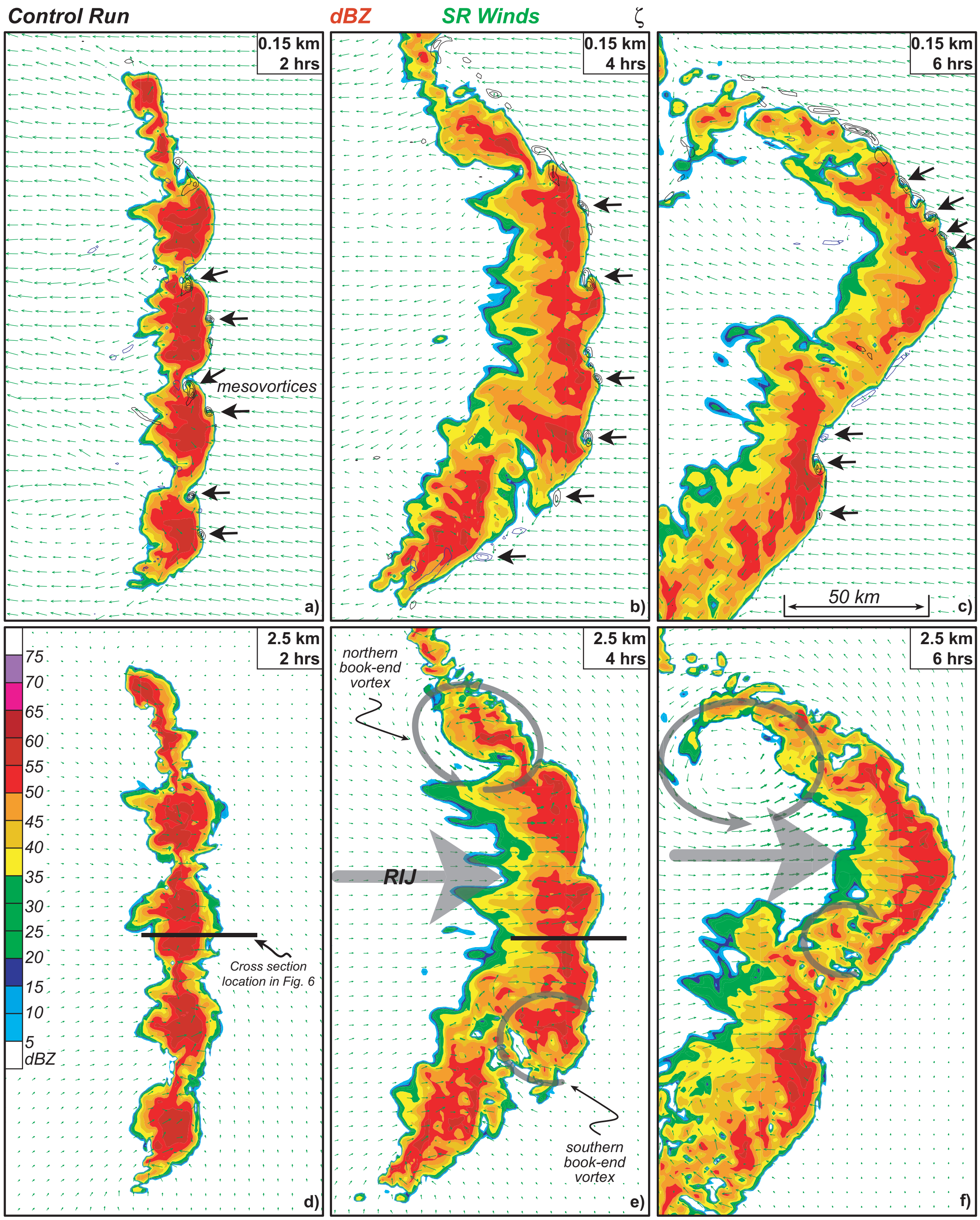

Figure 2. Simulated radar reflectivity (dBZ) in color along with storm-relative winds (ms^{-1}, green) and vertical vorticity (x10^{-3} s^{-1}, black) at 2, 4, and 6 hours. Data at 0.15 km and 2.5 km are shown in a-c and d-f, respectively. Locations of prominent meosvortices at 0.15 km are shown with black arrows.

the control run is presented in section 3 while section 4 shows the impact of stable layers on bow echo evolution. Conclusions are discussed in section 5.

2. MODEL FORMULATION AND EXPERIMENTAL DESIGN

In this study, the ARW model was used essentially as an idealized cloud model. Simulations six hours in length were carried out on a computational grid 350km x 370 km x 17.5 km in the x, y, and z directions, respectively. The horizontal grid spacing was 1 km. In the vertical, the grid spacing varied from 160 m near the lower boundary to 700 m at the top of the model domain. The lower boundary condition was free slip. The x and y boundary conditions were open. Microphysical processes were parameterized with the Kessler warm rain scheme. Sub grid turbulence was parameterized with the 1.5 TKE closure scheme and the coriolis forcing was set to 1×10^{-4} s^{-1}.

In the control run, the model domain was initialized with the sounding used by Weisman (1993). This sounding features 2377 J kg^{-1} of convective available potential energy (CAPE). The winds were westerly everywhere in the model domain increasing in strength from 0 to 20 ms^{-1} over the lowest 2.5 km AGL. The winds were constant above 2.5 km AGL and equal to 20 ms^{-1}.

Convection is initiated in the center part of the model domain by introducing four thermal bubbles spaced every 40 km in the north-south direction. The bubble perturbation was 3 K.

Stable layers were introduced into the model in two ways. The first set of experiments was meant to replicate the initiation and evolution of nocturnal, and perhaps elevated convection. Therefore, the stable layer was placed everywhere in the model domain (Fig. 1c). The stable layer depth was either 165m or 333 m AGL deep (Fig. 1a). The potential temperature deviation from the control run at the lowest grid point varied from 3 K to 11 K within the stable layer. In the second set of experiments, the stable layer was placed only in the eastern portion of the model domain (hereafter referred to as the RHS experiments). The transition zone width (Fig. 1b) from the ambient to the cool stable layer air was 10 km. The stable layer depths and strengths were the same as in the first set of experiments. The storm-relative base state flow would then advect the stable layer westward, towards the developing convective system. It would reach the leading edge of the developing bow echo by 2.5 hours into the simulation.

3. OVERVIEW OF CONTROL RUN

The evolution of the initiated convective system formed in the absence of a stable layer is shown in Fig. 2. Two hours into the simulation (Figs. 2a, 2d), the system is comprised of four primary areas of convection that have developed from the four thermal bubbles used to initiate the convection. At 0.15 km, mesovortices are observed along the leading edge of the convective system as relative maximum in the vertical vorticity field. Only positive circulations were observed at this time. Two hours later (Figs. 2b, 2e), the system has evolved into a well-defined bow echo. System-scale features such as the bookend vortices (Weisman 1993) and the RIJ are clearly evident at 2.5 km. The RIJ has descended to the ground producing storm relative winds in excess of 20 ms^{-1} (not shown). Prominent mesovortices are again evident at 0.15 km. Note that the stronger mesovortices seem to be located along the portion of the gust front that is being influenced by the RIJ. This observation is similar to those of Atkins et al. (2005) who showed that stronger, tornadic mesovortices formed along the bow echo gust front that had been strengthened by the RIJ.

By six hours into the simulation, the bow echo has evolved into an asymmetric structure with a stronger, more prominent northern bookend vortex (Fig. 2f). Mesovortices are still evident along the leading edge at 0.15 km.

A more complete illustration of mesovortex production and evolution within the control run can be seen in Fig. 3 where the tracks of most all mesovortices formed within the control run are highlighted. The first mesovortex formed 70 minutes into the simulation. Thereafter, mesovortices were observed out to six hours. A total of 33 mesovortices were identified having lifetimes of varying from 20 minutes to over four hours. Notice that two negative circulations formed within the convective system.

4. STABLE LAYER IMPACT ON DAMAGING SURFACE WINDS

In this section, the impact of low-level stable layers on the generation of strong surface winds within simulated bow echoes is examined. For brevity, only results from the RHS experiments, where the stable layer was placed in the right-hand side (eastern) portion of the domain, are presented herein. As discussed in section 2, the stable layer was advected by the storm-relative base state flow westward and subsequently interacted with the developing bow echo 2.5 hours into the simulation.

a. Impact on maximum surface winds

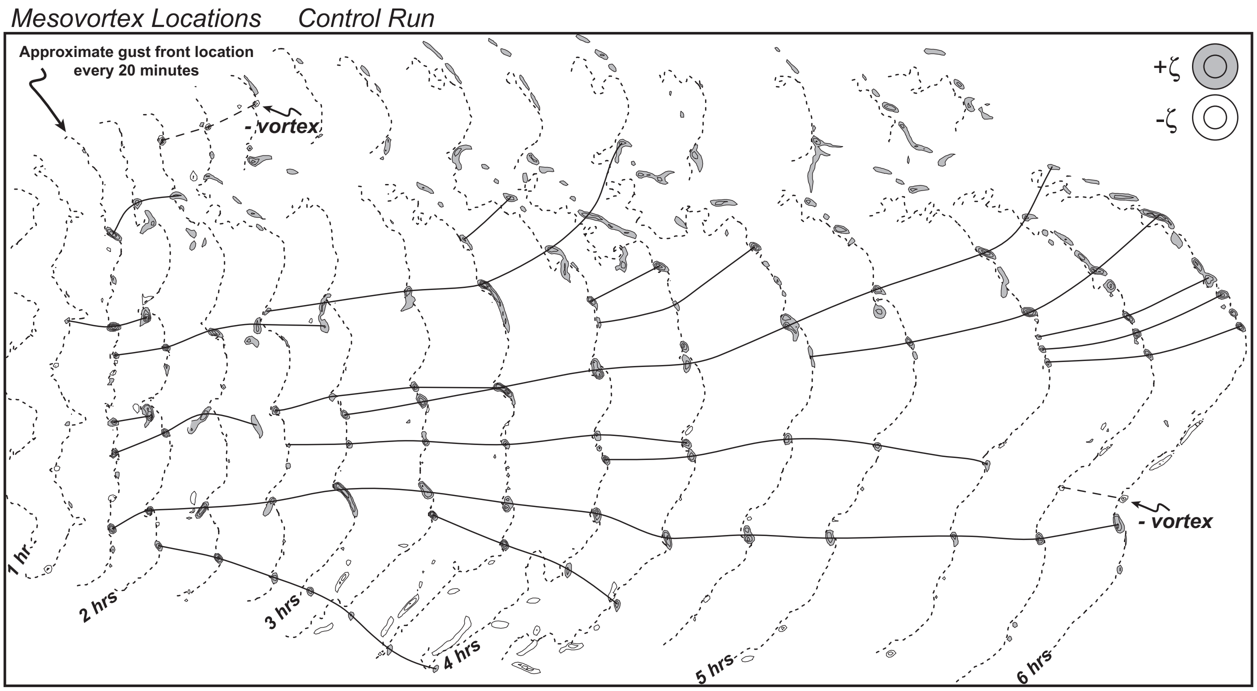

Figure 3. Gust front locations for the control run are plotted every 20 minutes beginning one hour into the simulation and ending at six hours. The gust front location is approximated by the 35 dBZ echo contour at 0.15 km. Vertical vorticity (black contours) is also shown indicating the locations of mesovortices. The shaded circulations are positive. Two negative circulations are also indicated. Thin black lines delineate mesovortex tracks.

The influence of stable layers on surface wind speeds is shown in Fig. 4 where the maximum u component of the wind (u_{max}) at the lowest grid level is plotted versus time for the control and stable layer runs. Since the convective system motion was westerly, u_{max} well-approximates the maximum wind speeds observed at the lowest grid location. A normalized ΔT ($n\Delta T$) value characterizes each stable layer run and is defined as $\frac{\theta'_{vsl}}{\theta'_{vcp}}$ at 2.5 hours into the simulation where $\theta_v'_{sl}$ represents the virtual potential temperature deficit within the stable layer and $\theta_v'_{cp}$ is the virtual potential temperature deficit within the developing cold pool. The $n\Delta T$ value provides a measure of the stable layer strength relative to the developing cold pool. The 2.5 hour time was chosen since this represents the time when the stable layer just begins to interact with the developing bow echo.

Within the control run, u_{max} values exceed 20 ms^{-1} after 3.5 hours into the simulation. At this time, the RIJ has developed and is descending to the ground (not shown) and mesovortices are present. When a stable layer in present, notice that the u_{max} values are quite similar to each other for all runs prior to the interaction with the stable layer at 2.5 hours. For $n\Delta T$ = 0.33, the evolution of u_{max} is not much different than the control after 2.5 hours. However, regardless of the stable layer depth, as the $n\Delta T$ value becomes larger and approaches 1, the u_{max} values drop off dramatically after 2.5 hours. When $n\Delta T$ = 1 or 1.2, u_{max} has fallen off by over a factor of two after the bow echo interacts with the stable layer. In comparing Figs. 4a and 4b, there is also a suggestion that deeper stable layers have a larger impact on u_{max} for the same $n\Delta T$. The results in Fig. 4 clearly show that stable layers influence the strength of surface winds formed within bow echoes. As previous work has shown that the damaging winds may be produced by either a descending RIJ or mesovortices, we now examine the impact of stable layers on mesovortex formation and evolution of the RIJ.

b. Stable layer influence on mesovortices

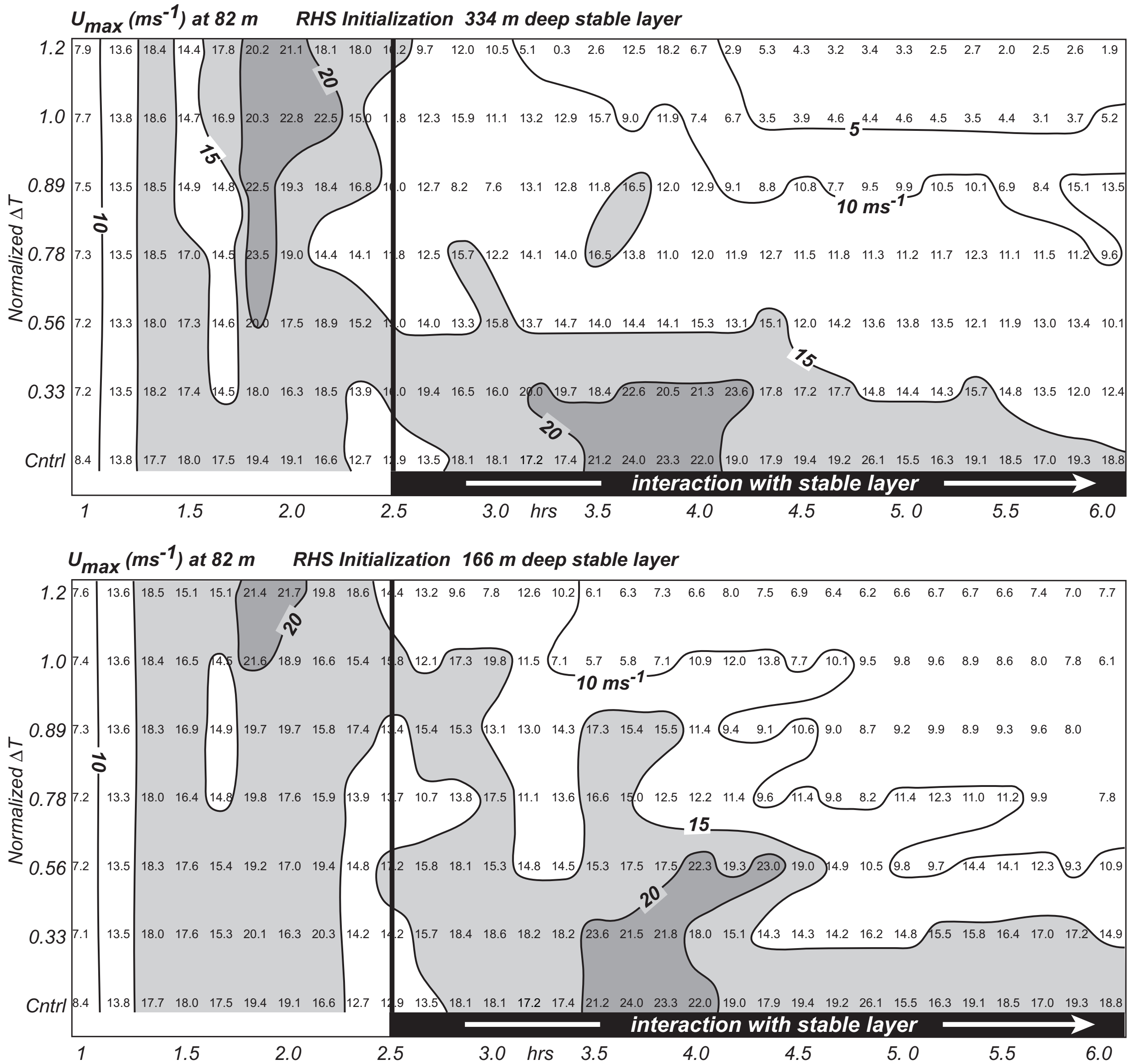

Figure 4. Maximum u component of the storm relative wind speed at the lowest grid level (82 m) for the control run along with stable layer simulations. (a) Stable layer depth of 334 m. The normalized ΔT value is defined in the text. (b) Same as in (a) but for 166 m deep stable layers.

The impact of the 165 m deep stable layer with nΔT = 1.2 on mesovortex evolution is shown in Fig. 5. Prior to 2.5 hours, mesovortex formation and evolution was very similar to that of the control run (Fig. 3). However, once the stable layer began to interact with the convective system, all existing mesovortices quickly dissipated. For example, the southern most vortex in the control run (Fig. 3) that initiated at 1 hour, 40 minutes persisted throughout the duration of the simulation. However, this same vortex in Fig. 5 weakened dramatically after 2.5 hours and dissipated one half hour later. Furthermore, no new mesovortices formed after 2.5 hours whereas mesovortices readily formed within the control run after this time. Thus, the stable layer appears to suppress the

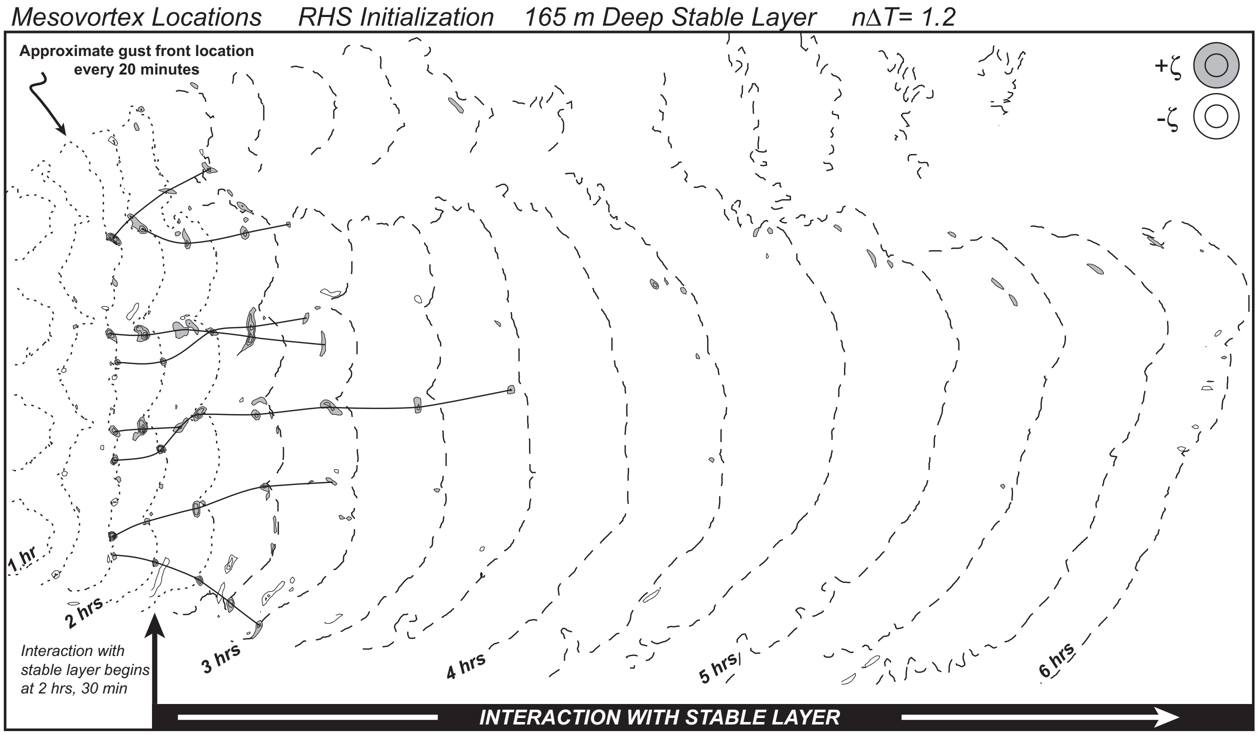

Figure 5. Same as in Fig. 3 except for the RHS initialization run with nΔT = 1.2.

generation of mesovortices at low levels. This behavior was observed progressively to a lesser extent in the other experiments as the stable layer strength became weaker (smaller nΔT values).

c. Stable layer influence on the RIJ

To examine the influence of stable layers on the RIJ and whether or not it is able to descend to the ground, vertical cross sections illustrating the RIJ structure for the control and RHS nΔT = 1.2 runs are now examined. A cross section through the apex of the developing bow echo at 2 hours into the simulation (Figs. 2a, d) is shown in Figs. 6a and b. In Fig. 6a, the air parcel trajectories show the inflow air moving to the west and ascending into the updraft at the leading edge of the gust front. In doing so, these air parcels transport the low-level higher θ_e air upward in the updraft. Behind the gust front, air parcel trajectories originating from 3-4 km are descending to the lowest grid levels. The slope of the trajectories suggest that the air parcels are descending more in convective-scale downdrafts rather than a mature RIJ. This result is consistent with the results in Fig. 2 that show localized RIJs just beginning to form within the convective system. This is also illustrated in Fig. 6b where only weak westerly flow is observed at mid levels behind the leading edge of the convective system. Fig. 6a also shows that the air parcels behind the gust front are transporting low θ_e air less than 328K from mid levels to the surface. The diverging nature of the trajectory paths at low levels is consistent with the presence of an area of high pressure at low levels centered at about 10 km. This high-pressure dome is generated by the cool, negatively buoyant air in the downdraft. The associated divergence is partially responsible for producing about 5 ms^{-1} of storm-relative flow at the lowest grid level behind the gust front (Fig. 6b).

Two hours later (Figs. 6c and d), one can again see the inflow parcels moving westward (Fig. 6c), ascending into the updraft, and transporting higher θ_e air upward. The air parcels behind the gust front are now descending within a well-developed RIJ to the lowest grid level, transporting low θ_e air less than 328 K to the surface from mid levels. The storm-relative *u* component of the flow exceeds 20 ms^{-1} at mid levels (Fig. 6d). The are parcel trajectories are transporting this higher momentum air to the surface where now 10 ms^{-1} of westerly

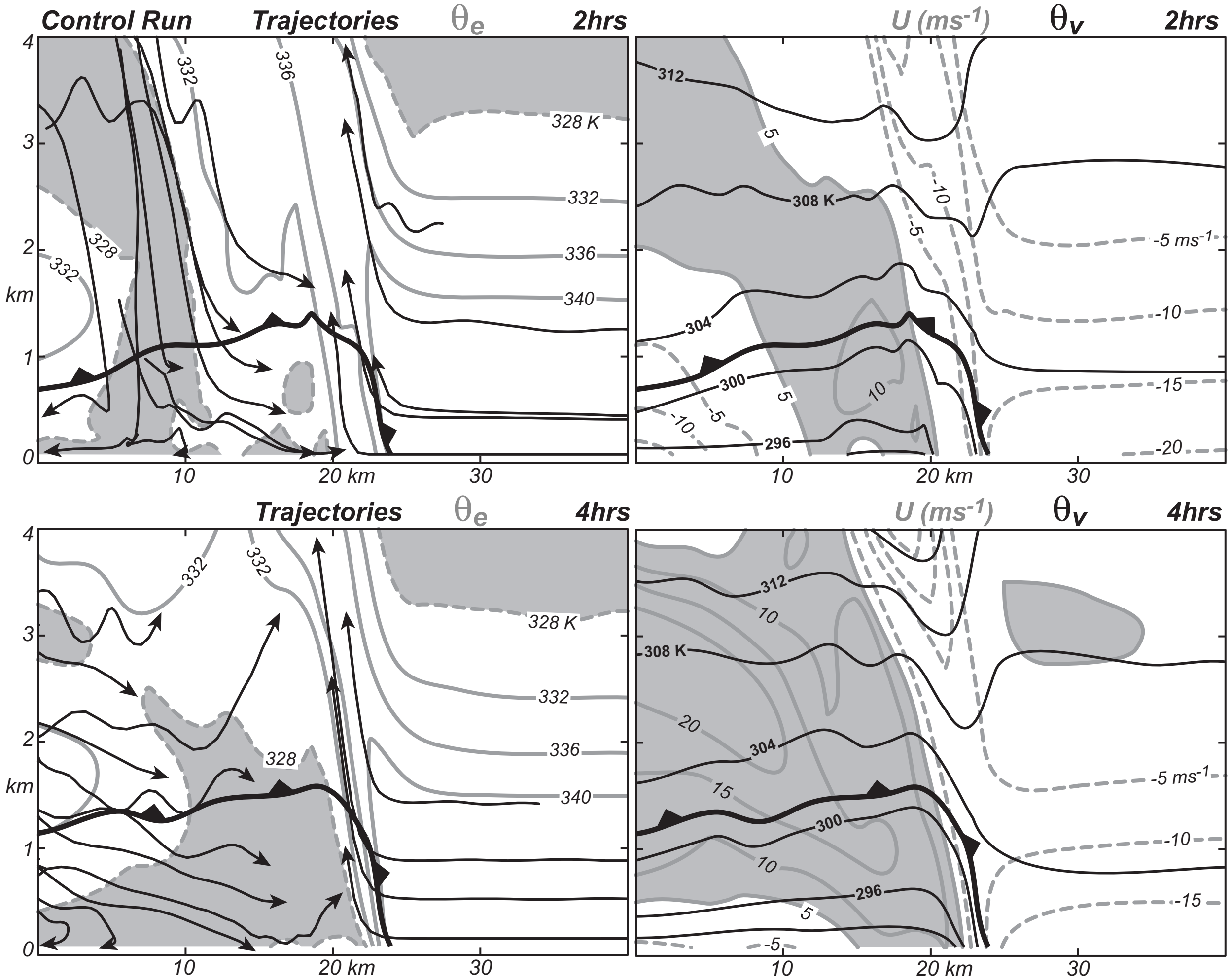

Figure 6. Vertical cross section through the control run at two and four hours. The cross section locations are shown in Fig. 2d and 2e. In panels (a) and (c), backward calculated air parcel trajectories are plotted in black. The arrow head corresponds to the parcel position at the respective time. Equivalent potential temperature (θ_e) is plotted in gray with values less than 328 K shaded and dashed. Panels (b) and (d) show virtual potential temperature (θ_v) in black and the u component of the wind contoured in gray with values greater than 5 ms^{-1} shaded. Negative values are dashed. In all panels, the approximate position of the gust front is delineated as a thick black line. All fields have been averaged over a distance of 10 km in the north-south direction.

flow is now observed behind the gust front. Note that the magnitudes of the fields shown in Fig.6 are likely underestimated due to the along-line averaging in the analysis. Divergence within the cold pool is again evident.

The results in Fig. 6 are to be compared with those in Fig. 7 where the convective system interacts with a stable layer. Two hours into the simulation (Figs. 7a and b), the flow structure is very similar to that in Fig. 6. Recall that the developing bow echo has yet to interact with the stable layer at this time. By four hours, however, the flow structure is very much different than in the control run. One can again see westward moving inflow parcels of air originating above the stable layer ascend in the updraft at the leading edge of the gust front, transporting higher θ_e air aloft. However, inflow parcels of air at low levels originating in the stable layer do not ascend into the updraft. Rather, they move at low levels into the vicinity of the bow echo cold pool. Notice that the θ_e values within the stable layer are 324 K or less. Behind the gust front, a RIJ is apparent, however, it has not

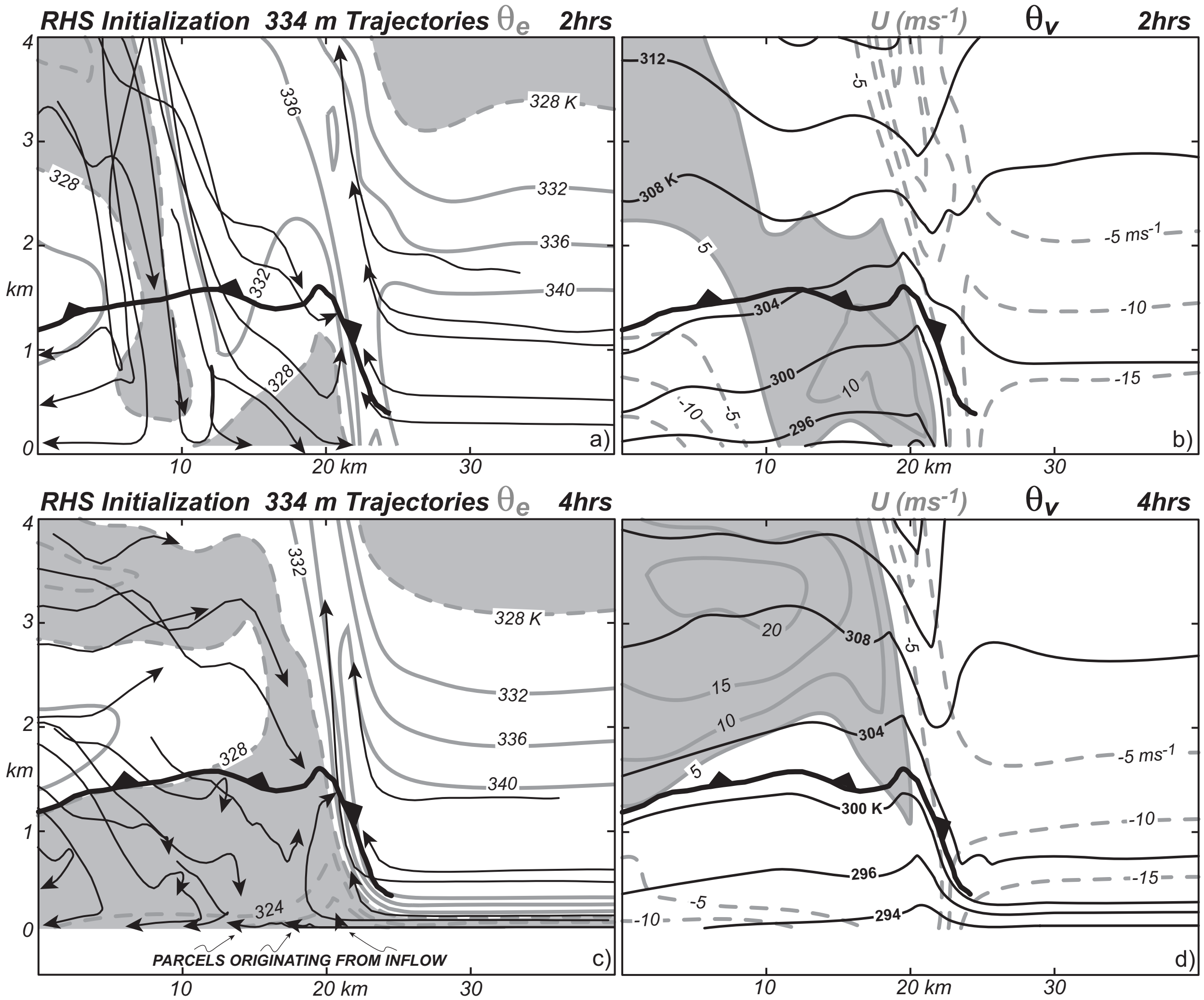

Figure 7. Same as in Fig. 6 but for the RHS nΔT = 1.2 run. The cross section location is at the apex of the bow echo. and is oriented west-east (not shown).

descended to the surface. Air parcels within the RIJ descend, but remain above those parcels at low levels that originated within the stable layer. Also notice that most all of the air parcels within the RIJ have θ_e values larger than those at low levels within the stable layer. Moreover, the θ_v field shows the potentially coolest cold pool air with values less than 294 K originated in the inflow. Thus, for stronger stable layers, the gust front no longer acts as a material surface at low levels. Potentially cooler, lower θ_e air in the stable layer is able to undercut the gust front. This air will then inhibit the RIJ from descending to the surface behind the leading edge of the bow echo, reducing the wind damage potential of the bow echo.

5. CONCLUSIONS

Idealized simulations of bow echoes interacting with low-level stable layers have been presented. It has been shown that the stable layer can reduce the damaging potential of a bow echo in two ways. First, the stable layer has been shown to mitigate the formation and evolution of mesovortices observed along the gust front. The reason why the mesovortices do not appear to form at low levels when a strong stable layer is present is currently under investigation. Second, strong stable layers inhibit the RIJ from descending from the ground if the surface θ_v of the stable layer is less than what is observed in the cold pool. In this case, low-level parcels from the inflow undercut the bow echo gust front. This descending, potentially cooler air inhibits air within the RIJ to reach the surface, a result also confirmed in trajectory and θ_e analyses. Current and future work is focussed in two areas. First, simulations are underway examining the impact of event deeper stable layers on bow echo evolution. Second, analyses of the simulations with weaker stable layers (e.g., nDT = 0.33-0.89) are underway to better understand what physical mechanisms are reducing the damaging surface winds in these simulated bow echoes (Fig. 3).

Acknowledgements: The research results presented herein were supported by the National Science Foundation under Grant ATM-0233178 and Vermont EPSCoR EPS-0236976.

References

Atkins, N.T., J.M. Arnott, R.W. Przybylinski, R.A. Wolf, and B.D. Ketcham, 2004: Vortex structure and evolution within bow echoes. Part I: Single-Doppler and damage analysis of the 29 June 1998 Derecho. *Mon. Wea. Rev.*, **132**, 2224-2242.

______, C.S. Bouchard, R.W. Przybylinski, R.J.Trapp, and G. Schmocker, 2005: Damaging surface wind mechanism within the 10 June 2003 Saint Louis bow echo during BAMEX. *Mon. Wea. Rev.*, **133**, 2275-2296.

Fujita, T.T., 1978: Manual of downburst identification for project Nimrod. Satellite and Mesometeorology Research Paper 156, Dept. of Geophysical Sciences, University of Chicago, 104 pp. [NTIS PB-286048]

______, 1979: Objectives, operation, and results of project NIMROD. Preprints, *11th Conf. on Severe Local Storms*, Kansas City, MO, Amer. Meteor. Soc., 259-266.

Jorgensen, D.P., H.V. Murphey, and R.M. Wakimoto, 2006: Rear-inflow structure in severe and non-severe bow-echoes observed by airborned Doppler radar during BAMEX. Preprints, *11th Conf. on Mesoscale Processes,* Albuquerque, NM, Amer. Meteor. Soc.

Przybylinski, R.W., G.K. Schmocker, and Y-J. Lin, 2000: A study of storm and vortex morphology during the ‘intensifying stage’ of severe wind mesoscale convective systems. Preprints, *20th Conf. on Severe Local Storms,* Orlando, FL, Amer. Meteor. Soc., 173-176.

Skamarock, W. C., J. B. Klemp, J. Dudia, D. O. Gill, D. M. Barker, W. Wang, and J. G. Powers, 2005: A description of the Advanced Research WRF version 2. NCAR Tech. Note NCAR/TN-468+STR, 100 pp.

Trapp, R.J. and M.L. Weisman, 2003: Low-level mesovortices within squall lines and bow echoes. Part II: Their genesis and implications. *Mon. Wea. Rev.*, **131**, 2804-2823.

Wakimoto, R.M., H.V. Murphy, A. Nester, D.P. Jorgensen, and N.T. Atkins, 2006: High winds generated by bow echoes. Part I: Overview of the Omaha bow echo 5 July 2003 storm during BAMEX. Accepted to *Mon. Wea. Rev.*

______, H.V. Murphy, C.A. Davis, and N.T. Atkins, 2006: High winds generated by bow echoes. Part II: The relationship between the mesovortices and damaging straight-line winds. Accepted to *Mon. Wea. Rev.*

Wheatley, D.M., R.J. Trapp, and N.T. Atkins, 2006: Radar and damage analysis of severe bow echoes observed during BAMEX. *Mon. Wea. Rev.*, **134**, 791-806.